

# A theoretical view on self-assembled monolayers in organic electronic devices

Georg Heimel<sup>\*a,d</sup>, Lorenz Romaner<sup>b</sup>, Egbert Zojer<sup>c</sup>, and Jean-Luc Brédas<sup>d</sup>

<sup>a</sup>Institut für Physik, Humboldt Universität zu Berlin, Newtonstr. 15, D-12489 Berlin, Germany;

<sup>b</sup>Department of Material Physics, University of Leoben,  
Erzherzog-Johann Strasse 3, A-8700 Leoben, Austria;

<sup>c</sup>Institute of Solid State Physics, Graz University of Technology,  
Petersgasse 16, A-8010 Graz, Austria;

<sup>d</sup>School of Chemistry and Biochemistry and Center for Organic Photonics and Electronics,  
Georgia Institute of Technology, Atlanta, GA 30332-0400, USA

## ABSTRACT

Self-assembled monolayers (SAMs) of covalently bound organic molecules are rapidly becoming an integral part of organic electronic devices. There, SAMs are employed to tune the work function of the inorganic electrodes in order to adjust the barriers for charge-carrier injection into the active organic layer and thus minimize undesired onset voltages. Moreover, in the context of molecular electronics, the SAM itself can carry device functionality down to a few or even a single molecule. In the present contribution, we review recent theoretical work on SAMs of prototype  $\pi$ -conjugated molecules on noble metals and present new data on additional systems. Based on *first-principles* calculations, we establish a comprehensive microscopic picture of the interface energetics in these systems, which crucially impact the performance of the specific device configuration the SAM is used in. Particular emphasis is put on the modification of the substrate work function upon SAM formation, the alignment of the molecular levels with the electrode Fermi energy, and the connection between these two quantities. The impact of strong acceptor substitutions is studied with the goal of lowering the energy barrier for the injection of holes from a metallic electrode into the subsequently deposited active layer of an organic electronic device.

**Keywords:** Self-assembled monolayer, density-functional theory, work function, level alignment, interfaces, organic electronics, molecular electronics

## 1. INTRODUCTION

Monolayers of organic molecules covalently bound to a multitude of substrates have attracted considerable interest over the past years.<sup>1, 2</sup> The spontaneous self-assembly of suitable molecules into densely packed and often ordered layers makes this approach highly suitable for modifying macroscopic surface properties such as, e.g., wetting<sup>3</sup> or corrosion resistance,<sup>4</sup> and a number of applications has been proposed for such *self-assembled monolayers* (SAMs).<sup>5-11</sup> Notably, SAMs are employed in organic electronic devices, e.g., organic light-emitting diodes (OLEDs) or organic field-effect transistors (OFETs), in order to control, among other parameters, the energetics at the interface between the inorganic electrodes and the active organic layer.<sup>12-20</sup>

The nature and the importance of the interface energetics in such structures are demonstrated in Figure 1. There, a simplified schematic of the electrode/organic contact regions is shown for a generic device architecture in Figure 1a. At the anode, holes are injected into the occupied states of the organic semiconductor where they are stabilized by polarizing surrounding matter and locally distorting the organic lattice; a positive *polaron*,  $P^+$ , is formed that travels through the organic semiconductors under the influence of an external (or built-in) electric field. The energetic offset between the anode Fermi level ( $E_F$ ) and the electronic bands derived from the highest occupied molecular orbitals

\* E-Mail: georg.heimel@physik.hu-berlin.de

(HOMO) of the molecules in the organic layers is commonly termed *hole-injection barrier* (HIB). At the cathode, a similar scenario is encountered for electrons; after injection, negative polarons,  $P^-$ , are formed as the principal charge carriers. Correspondingly, the energetic mismatch between the cathode  $E_F$  and the electronic bands derived from the lowest unoccupied molecular orbitals (LUMO) is often referred to as the *electron-injection barrier* (EIB).<sup>21</sup>

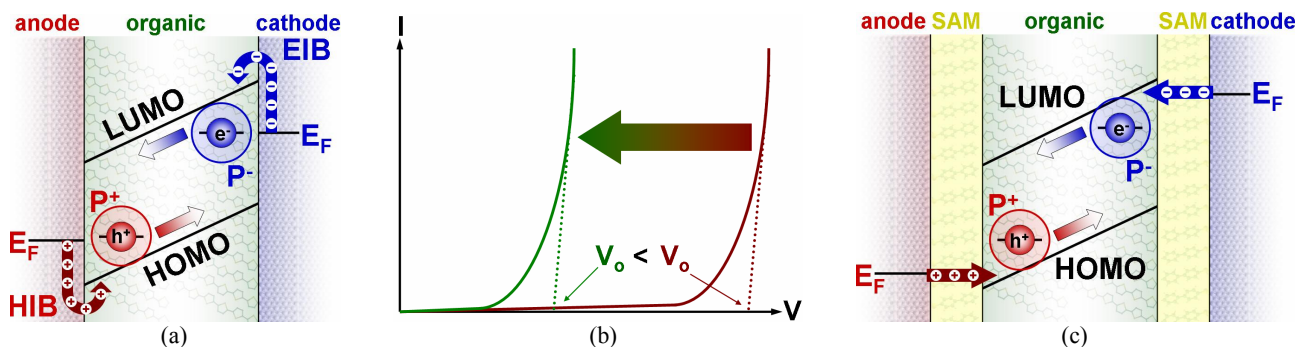


**Fig. 1.** Schematic illustrating the energetics at the electrode/organic interfaces typically encountered in organic electronic devices. (a) Holes ( $h^+$ ) need to overcome the hole-injection barrier (HIB) at the anode, i.e., the energetic offset between the anode Fermi level ( $E_F$ ) and the HOMO, before positive charge carriers ( $P^+$ ) can flow through the device. Electrons ( $e^-$ ) need to overcome the electron-injection barrier (EIB) between the cathode  $E_F$  and the LUMO before negative charge carriers ( $P^-$ ) can start to flow. (b) Schematic current-voltage (IV) characteristics of an organic diode structure containing the interfaces shown in (a).  $V_o$  denotes the onset voltage determined by the height of the charge-carrier injection barriers, red for higher barriers and green for lower barriers. (c) Modification of the electrodes with suitable dipolar SAMs reduces the injection barriers by increasing [decreasing] the anode [cathode] work function.

Charge carriers need to overcome these energy barriers before current can flow through the device which gives rise to undesirable onset voltages,  $V_o$ , below which the device remains inactive. A schematic current-voltage (IV) curve of an organic diode structure containing such interfaces is drawn in Figure 1b (red line). For improved performance of such devices, it is crucial to both reduce and balance the charge-carrier injection barriers. In the past, this has been achieved by matching the work function,  $\Phi$ , of the electrodes with the energy of the respective transport levels in the organic, i.e., high- $\Phi$  materials for the anode and low- $\Phi$  materials for the cathode. Recently, however, SAMs of dipolar molecules have been used to tune  $\Phi$  of typical electrode materials<sup>12-20</sup> and, thus, considerably reduce the charge-carrier injection barriers (Figure 1c). The consequence for the IV-characteristics of such an improved diode structure is shown in Figure 1b (green line);<sup>12, 17, 20</sup>  $V_o$  is considerably reduced, resulting in lower driving voltages necessary to achieve comparable device performance, i.e., lower power consumption.

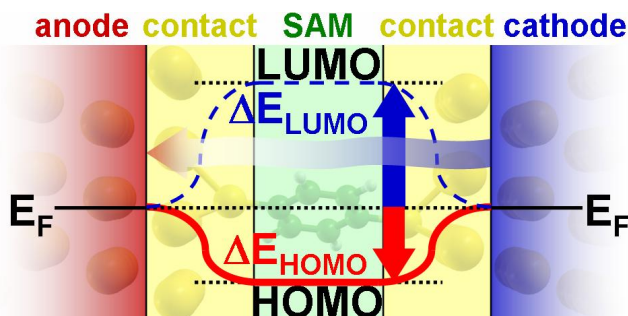


**Fig. 2.** Schematic illustrating the interface energetics in a single molecule junction. The energetic separations ( $\Delta E_{HOMO}$  and  $\Delta E_{LUMO}$ ) between the metal Fermi level ( $E_F$ ) and the frontier molecular orbitals (HOMO and LUMO) impact the effective tunnel barrier for charge transport through the junction. In particular, the molecular level closer to  $E_F$  is related to the effective barrier height (red line).

The spontaneous self-assembly of organic molecules onto a suitable (metallic) electrode structure also forms the basis for the entire field of *molecular electronics*, where the interfaces essentially are the devices. Depending on the resolution

of lateral structuring, either a macroscopically extended SAM can carry device functionality<sup>22, 23</sup> or a few and even a single molecule can work as a functional unit.<sup>24-28</sup> Here, the situation is very similar to the interface energetics in (macroscopic) organic electronic devices, only the relevant length scale shrinks from molecular to atomic dimensions. As depicted in Figure 2, it is now the alignment ( $\Delta E_{HOMO}$  and  $\Delta E_{LUMO}$ ) of the electrode  $E_F$  with the frontier molecular orbitals of the SAM itself that determines the charge-transport characteristics through such a molecular junction. In particular, the energetic position of the molecular orbital closer to  $E_F$  (the HOMO in Figure 2) determines the effective barrier height for the tunneling process through the molecule(s).<sup>29-34</sup> Reminiscent of the role SAMs played at interfaces in organic electronics (Figure 1), details in the chemical binding at the metal/molecule contact now determine the level alignment between the electrodes and the active part of the device and, consequently, its IV-characteristics.<sup>29-34</sup>

In the present contribution, we strive to establish a comprehensive microscopic picture of the interface energetics in this important class of systems that determine the most relevant parameters for their use in organic and molecular electronic devices. To that end, we extend our recent theoretical work,<sup>35-42</sup> based on *first-principles* calculations and electrostatic considerations, to novel systems. The physisorption of conventional organic semiconductors, SAMs, or simply non-specific organic contaminants tends to lower the metal work function and, thus, naturally increases the HIB (Figure 1).<sup>43, 44</sup> Only few approaches have been proposed to increase the metal work function and, thus, lower the HIB. In particular, oxidation of the gold surface,<sup>45</sup> strong acceptor molecules,<sup>46, 47</sup> or SAMs of fluorinated alkanethiols<sup>13, 14, 48</sup> or fluorinated oligo(*para*-phenylene-ethynylene)s<sup>12, 19</sup> have been proposed. Here, we focus on SAMs of 4'-X-4-mercaptobiphenyl on Au(111), where X is a strongly electronegative group, i.e., -NO<sub>2</sub> as an extreme and -F as a more realistic example, and we find that both can be expected to significantly decrease the HIB at the contact between metal and organic semiconductor.

## 2. METHODOLOGY

In the present study, we focus on two different SAMs on Au(111), one composed entirely of 4'-nitro-4-mercaptobiphenyl and the other of 4'-fluoro-4-mercaptobiphenyl. For reasons of consistency, both molecules are assumed to form close-packed SAMs with two molecules in a lateral  $p(\sqrt{3}\times 3)$  surface unit cell arranged in the typical *herringbone* pattern.<sup>49, 50</sup> Thiols are assumed to adsorb upon hydrogen abstraction. In the lack of concise experimental evidence for these systems, no major gold reconstruction (e.g., ad-atoms)<sup>51-57</sup> has been taken into account. For this situation, we find, in accordance with previous theoretical studies,<sup>58-65</sup> the *fcc*-hollow as the most favorable adsorption site for the sulfur. The long molecular axes are found to be inclined to the surface normal by an angle  $\theta \approx 12^\circ$ .

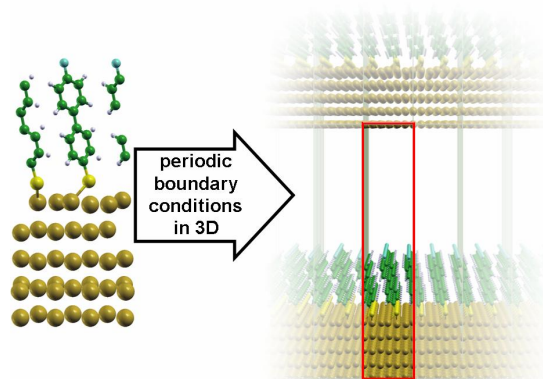


**Fig. 3.** Illustration of the repeated slab approach. The 2D unit cell containing 5 gold layers and 2 molecules adsorbed on the top side is periodically repeated in all three dimensions. A vacuum gap separates consecutive images of 2D-periodic infinite slabs. The red rectangle marks the 3D unit cell and the fading indicates periodic repetition of the shown structure in the respective direction.

The computational methodology is described and benchmarked elsewhere.<sup>37</sup> Here, only a brief description is given: We performed spin-restricted density-functional theory calculations (with the PW91 exchange-correlation functional)<sup>66</sup> using the projector augmented-wave method<sup>67, 68</sup> for the description of the valence-core interaction, allowing for the low

kinetic-energy cutoff for the plane-wave expansion of the valence Kohn-Sham orbitals of 20 Ryd. In order to simulate a laterally extended surface, we employed periodic boundary conditions in the *repeated-slab* approach (Figure 3). 5 layers of gold were used to represent the Au(111) surface in the lateral unit cell described above (left panel in Figure 3). This unit cell is then periodically repeated in all three dimensions (right panel in Figure 3). Introducing a vacuum gap of  $>20$  Å above the molecules prevents spurious interactions between two consecutive images of the 2D-periodic, infinite slabs. All calculations were performed with the VASP code,<sup>69-72</sup> 3D graphics were produced with XCrysDen.<sup>73</sup>

### 3. RESULTS AND DISCUSSION

#### 3.1 Isolated molecular layers

Prior to focusing on the metal/molecule bond formation, it is useful to look in more detail at the molecular part of the system. To that end, some important concepts are first established for an isolated (no metal present), free-standing layer of molecules. The atomic positions in this layer are frozen to the equilibrium geometry optimized for the layer adsorbed on Au(111). The following discussion will deal with the  $-\text{NO}_2$  substituted molecules only; the same consideration, however, hold for all 4<sup>+</sup>-substitutions.<sup>35-39, 41, 42</sup>

When conceptually partitioning the thiol-SAM/Au(111) system into the metallic and SAM part, the question about the chemical structure one should assume for the molecules arises. In a real-world scenario, the SAM forms from thiols, i.e., R-SH. Following a still disputed reaction pathway,<sup>74</sup> the hydrogen atom is abstracted during SAM formation and a covalent S-Au bond is formed, showing very little charge transfer between metal and sulfur.<sup>35-39, 41, 42</sup> Simply “cutting” this S-Au bond, would render the molecular part a neutral radical species (i.e., R-S•). While chemically, this is an unlikely step in the adsorption pathway, it is, as we shall see, a highly instructive conceptual intermediate which allows commenting on the nature of the S-Au bond and is commonly used in surface-theoretical studies.<sup>75, 76</sup> In the following, we will consider both scenarios: (i) the isolated freestanding molecular layer where the sulfur atoms are saturated with hydrogens (conceptually equivalent to the situation *before SAM adsorption*); and (ii) the isolated freestanding layer of radicals (conceptually equivalent to the situation *after SAM desorption*).

The molecules considered in the present study possess a strong dipole moment along their long molecular axes (pointing towards the thiol) due to the strong electron accepting character of the -F and, in particular, the  $-\text{NO}_2$  head-group substitution. Arranging the molecules in an ordered layer with aligned long molecular axes corresponds to the formation of a dipole layer. From basic electrostatic considerations, it is known that a 2D-infinite dipole layer causes a step in the electrostatic potential, dividing space into two regions where the electrostatic potential energy of an electron at rest,  $U_{\text{vac}}$ , is higher on the negative side of the dipole layer than on the positive side.

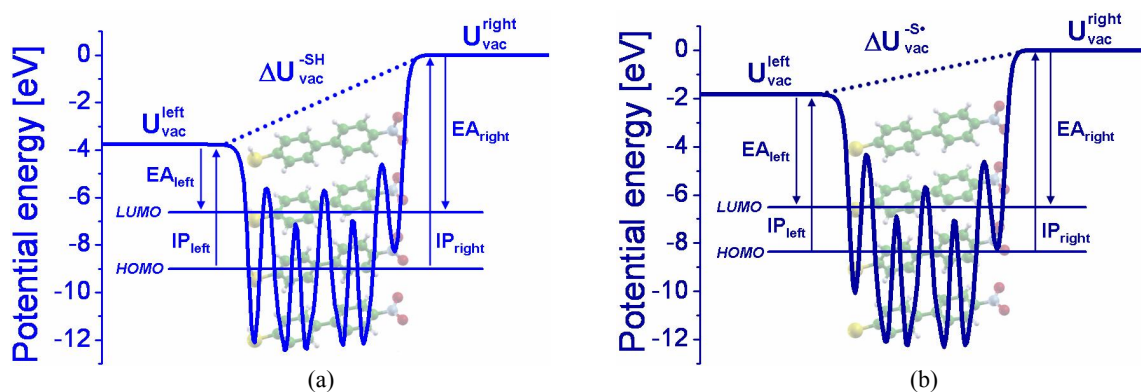


**Fig. 4.** Calculated electrostatic potential energy for electrons, averaged within the plane of the  $-\text{SH}$  (a) and  $-\text{S}^\bullet$  (b) terminated, freestanding  $\text{NO}_2$ -substituted molecular layers. Left and right denote the sulfur and  $-\text{NO}_2$  sides, respectively. The vertical lines indicate the calculated energetic positions of the maxima in the density of states corresponding to the (weakly dispersing) HOMO- and LUMO-derived bands. Arrows indicate the respective ionization potentials ( $IP$ ) and electron affinities ( $EA$ ).

In Figure 4a, the calculated electrostatic potential energy for electrons across the freestanding 4'-nitro-4-mercaptobiphenyl layer is shown, averaged within the plane of the layer. As expected,  $U_{vac}$  is higher on the (negative) -NO<sub>2</sub> side (right) than on the (positive) -SH side (left). The difference between  $U_{vac}^{left}$  and  $U_{vac}^{right}$ ,  $\Delta U_{vac}^{-SH}$  in this case, is, in principle, proportional to the projection of the molecular dipole moment onto the layer normal. Note, however, that the proportionality constant depends critically on the packing density of molecules in the SAM, the packing motif, as well as on details of the molecular (electronic) structure and the substituents.<sup>41</sup> This step in potential energy across the layer has an important implication: while in the case of a single isolated molecule, the ionization potential ( $IP$ ) [electron affinity ( $EA$ )] does not depend on the direction an electron is ejected to [added from], the situation is different for layers of dipolar molecules. As such a layer still has relatively well-defined frontier molecular orbitals (neglecting inter-molecular band dispersion), there is only one initial-state energy for an electron in an ionization process (approximated by the HOMO energy). However, the final-state energy of the ejected electron is now different ( $U_{vac}^{left}$  or  $U_{vac}^{right}$ ) depending on which side of the layer that electron comes to rest. Consequently, there are also two different ionization potentials,  $IP_{left}$  and  $IP_{right}$  (Figure 4). Similarly, for the electron affinity, there is only one final-state energy for the added electron (approximated by the LUMO energy) but two different initial-state energies,  $U_{vac}^{left}$  and  $U_{vac}^{right}$ . Thus, a dipolar molecular layer has two different electron affinities,  $EA_{left}$  and  $EA_{right}$ , and, as with  $IP_{left}$  and  $IP_{right}$ , the difference between left- and right-sided quantities is  $\Delta U_{vac}$ .<sup>21</sup>

For case (ii), the layer of R-S• radical, the plane-averaged  $U(z)$  is shown in Figure 4b.<sup>77</sup> The same considerations hold as in case (i). The different electron density on the sulfur (due to the unpaired electron) raises  $U_{vac}^{left}$ , also evident in the reduced depth of the sulfur-associated potential well compared to Figure 4a. Consequently, the step in the potential energy across the layer,  $\Delta U_{vac}$ , is smaller in case (ii) than in case (i) by ca. 1.9 eV.

### 3.2 Metal-molecule bond formation

In a second step, the mechanism of bond formation will now be discussed for the two cases introduced above: (i) bonding of R-SH to Au upon hydrogen abstraction and (ii) bonding of the R-S• species to Au. In the former, a covalent bond (S-H) is *replaced* by a different covalent bond (S-Au) while, in the latter, a new covalent bond is *formed* (S-Au). In order to visualize the flow of charge upon bond formation, the charge-density difference, i.e., the difference between the charge-density,  $\rho$ , of the full metal+SAM system (final state) and the sum of the densities of the isolated subsystems (initial state) is calculated. The latter is different for the two situations (i) and (ii): In case (i), it is composed of the charge density of the clean metal surface,  $\rho_{Au}$ , and that of the freestanding molecular monolayer,  $\rho_{SAM}$ , minus that of the hydrogen atoms,  $\rho_H$  (Equation 1a), whereas, in case (ii),  $\rho_H$  does not appear (Equation 1b). A 3D representation of these charge-density differences,  $\Delta\rho$ , is shown in Figure 5 for the 4'-nitro-4-mercaptobiphenyl.

$$\Delta\rho = \rho - [(\rho_{SAM} - \rho_H) + \rho_{Au}] \quad (1.a)$$

$$\Delta\rho = \rho - (\rho_{SAM} + \rho_{Au}) \quad (1.b)$$

Note that  $\Delta\rho$  necessarily includes contributions from the formation (replacement) of covalent bonds *and* the “push-back” effect.<sup>78-81</sup>

The respective left panels in Figures 5a and 5b (blue) mark regions of electron depletion upon metal-SAM bond formation and the respective right panels (red) indicate regions of electron accumulation. The first important observation is that the charge-density redistribution upon bond formation is strongly localized at the immediate metal/sulfur interface, even more so in case (i) than in case (ii). This leads to the important conclusion that, for densely packed SAMs of thiols, the bonding induced charge rearrangements are almost completely decoupled from the head-group substitution. In fact, while data is shown only for the -NO<sub>2</sub> substituted compound in Figure 5, it is virtually identical for other head-group substitutions,<sup>36-39, 41, 42</sup> in particular -F. Due to the superposition of hydrogen cleavage and S-Au bond formation in case (i),  $\Delta\rho$  in Figure 5a reveals little chemical insight. For case (ii) however,  $\Delta\rho$  in Figure 5b clearly shows that electrons flow from the  $\sigma$ -system on the molecule (bonding in the S-C region) into the  $\pi$ -system of the molecule (antibonding in the S-C region).<sup>37</sup>

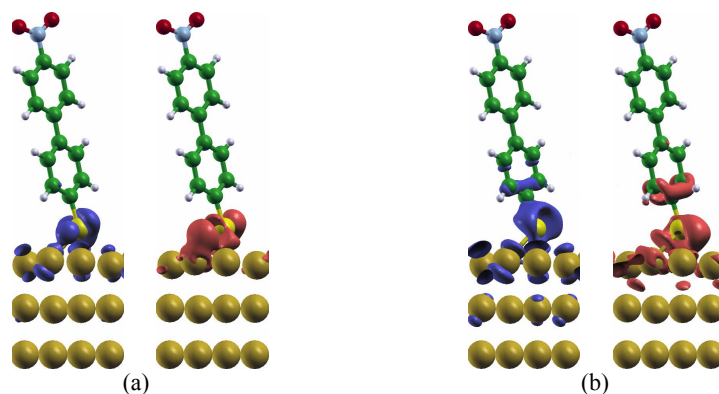


**Fig. 5.** Isodensity representation of the charge flow upon metal-SAM bonding in the case of 4'-nitro-4-mercaptobiphenyl. (a) Adsorption of R-SH including abstraction of hydrogen; (b) adsorption from the R-S• species. Blue (left panels) indicate regions of electron depletion and red (right panels) mark regions of electron accumulation.

More so than the details of  $\Delta\rho$  in three dimensions, the integrated (in the plane of the SAM, parallel to the surface) quantities are relevant for the interface energetics in these systems. In Figure 6, the integrated  $\Delta\rho$ ,  $\Delta\rho(z)$  is shown for 4'-nitro-4-mercaptobiphenyl in both cases, (i) and (ii). Again, regions of electron depletion are shaded in blue and regions of electron accumulation are highlighted in red. Importantly, Figure 6 indicates that no significant long-range charge transfer from metal to molecule or vice versa occurs. Only a slight shift of charge within the SAM is seen in the case of adsorption from R-S• (Figure 6b), where electrons flow from the region of the S-C bond into the region of the carbon atoms closest to the metal/molecule interface.

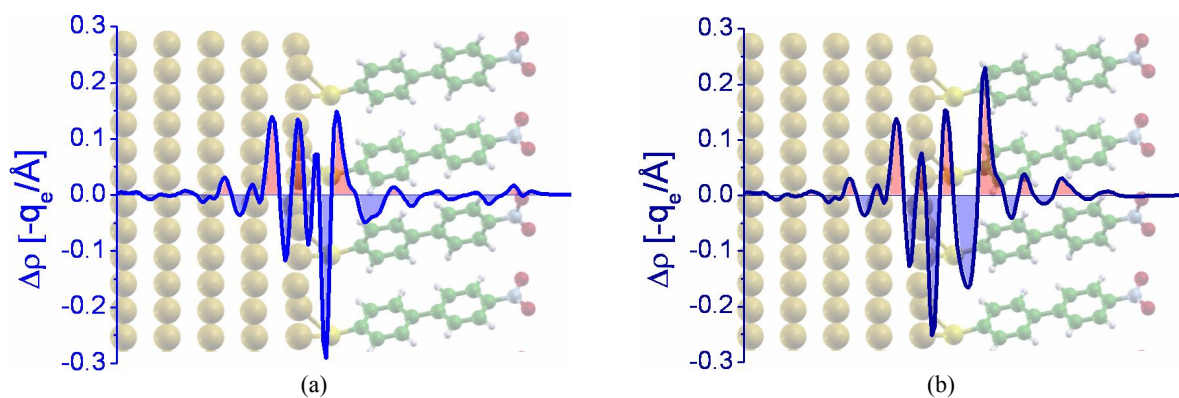


**Fig. 6.** Integrated charge-density difference,  $\Delta\rho(z)$ , upon SAM formation from the R-SH species (a) and the R-S• species (b). Regions of electron depletion are shaded in blue (negative values) and regions of electron accumulation are highlighted in red (positive values).

Solving the one-dimensional Poisson equation by integrating  $\Delta\rho(z)$  from Figure 6, yields a step in the electrostatic potential energy for electrons,  $\Delta U(z)$ , across the metal/SAM interface which, upon bond formation, shifts the potential well of the SAM (Figure 4) relative to that of the clean gold surface.<sup>35-39, 41, 42</sup> The respective  $\Delta U(z)$  for 4'-nitro-4-mercaptobiphenyl in both scenarios, (i) and (ii), are shown in Figure 7. Similar to  $\Delta\rho(z)$ , also  $\Delta U(z)$  is largely confined to the immediate metal/sulfur interface region with a tail extending into the first phenylene ring. We refer to the magnitude of the total step in potential energy as *bond dipole* ( $BD$ ).<sup>35-39, 41, 42</sup> Importantly, the shape of  $\Delta U(z)$  and the magnitude of  $BD$  are largely independent of the head-group substitution in densely packed SAMs. They do, however, strongly depend on the nature of the docking chemistry and may change in sign and magnitude when different docking groups (e.g., isocyanide or pyridine)<sup>38</sup> are used or when the substrate metal is changed to, e.g., silver.<sup>38, 39</sup> Interestingly,  $BD$  is of opposite sign for the two processes of SAM formation considered here (adsorption from R-SH and adsorption from R-S•) and the difference amounts to ca. 1.8 eV. Thus, care must be taken when comparing references in which different approaches to partitioning the SAM/metal system are used.<sup>36-38, 75, 76</sup>

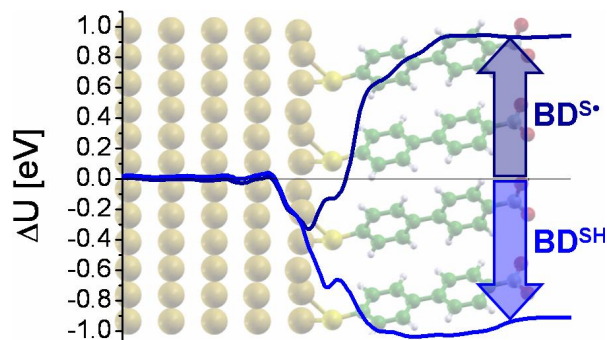


Fig. 7. Step in the electrostatic potential energy for electrons across the metal/molecule interface due to bonding-induced interfacial charge rearrangements; dark blue for adsorption from the R-S• species, light blue from the thiol (R-SH).

### 3.3 Work-function modification and level alignment

With all the individual contributions in place, a microscopic picture of the interface energetics in SAMs can now be established. The final level alignments and work functions of the SAM covered surfaces are summarized in Figure 8. Upon SAM formation, the work function of the clean gold surface,  $\Phi_{Au}$  (calculated to be 5.2 eV),<sup>37</sup> is modified. The magnitude of this work-function modification,  $\Delta\Phi$ , is determined by two additive contributions,  $\Delta U_{vac}$  (Figure 4) and  $BD$  (Figure 7).<sup>35-39, 41, 42</sup>

$$\Delta\Phi = \Delta U_{vac} + BD \quad (2)$$

An electron that is ejected from the metal through the SAM has to overcome two additional energy steps to reach the vacuum level on top of the SAM,  $U_{vac}^{right}$ . One,  $\Delta U_{vac}$ , is created by the dipolar molecular layer (Figure 4) and the other,  $BD$ , arises from the metal-molecule bond formation.<sup>35-39, 41, 42</sup>

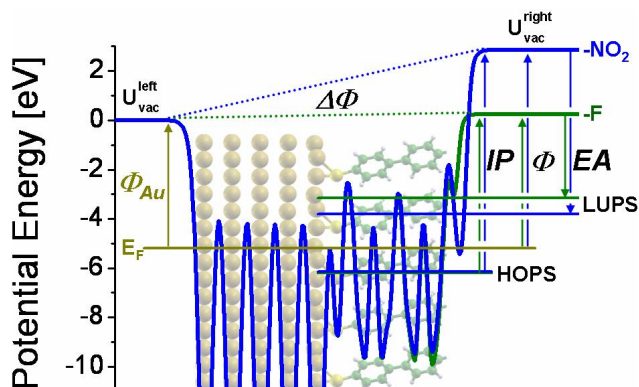


Fig. 8. Plane-averaged electrostatic potential energy for electrons across the metal/SAM interface for the NO<sub>2</sub><sup>-</sup> (blue) and F<sup>-</sup> (green) substituted molecules. The vertical lines mark the energetic position of the Fermi level ( $E_F$ ), the highest occupied  $\pi$ -states (HOPS) in the SAM, and the lowest unoccupied  $\pi$ -states (LUPS). The work function of the clean gold surface ( $\Phi_{Au}$ ), the modification thereof ( $\Delta\Phi$ ), the work function of the SAM-covered surface ( $\Phi$ ), as well as the ionization potential ( $IP$ ) and the electron affinity ( $EA$ ) of the SAM are also indicated.

It is important to note that, for the final situation depicted in Figure 8 (the SAM adsorbed on gold), the particular choice for the reaction pathway is, of course, irrelevant. The magnitude of  $\Delta\Phi$  must be independent of whether we conceptually regarded the process of SAM adsorption as the *replacement* of the S-H bond with the S-Au bond or as the *formation* of a bond between the radical R-S• species and the gold surface; the difference between  $\Delta U_{vac}^{-SH}$  and  $\Delta U_{vac}^{-S\bullet}$  (Figure 4) is fully compensated by the difference between  $BD^{SH}$  and  $BD^{S\bullet}$  (Figure 7).

A closer inspection of Figure 8 reveals that, in the case of the -NO<sub>2</sub> substituted SAM, the work function of the clean gold surface,  $\Phi_{Au}$ , is significantly increased, thus promoting a reduction of the hole-injection barrier (Figure 1) into a subsequently deposited organic semiconductor. Note, however, that the strong molecular dipoles, all aligned in parallel, repel each other for electrostatic reasons and, therefore, the close packing assumed for the present calculations might not be achievable in experiment. The scenario depicted in Figure 8 must thus be seen as an upper limit. For the -F substituted compound, 4'-fluoro-4-mercaptobiphenyl, we find that the work function of the SAM covered surface,  $\Phi$ , is approximately equal to that of  $\Phi_{Au}$  as  $\Delta U_{vac}$  and  $BD$  cancel each other in this case. However, the hole-injection barrier (HIB) from the metal into an organic semiconductor subsequently deposited on the SAM can still be expected to be smaller than without the SAM. This is because, when physisorbing organic molecules onto metals, the metal work function is generally reduced due to the push-back effect,<sup>43, 44, 78-81</sup> which is typically not the case when depositing organic molecules onto other organics.<sup>82</sup>

Concerning the energetic alignment of the frontier molecular orbitals in the SAM with  $E_F$ , it is important to note that, upon metal-SAM bond formation, the molecular-level derived bands hybridize with the metal and, consequently, are considerably broadened.<sup>38</sup> It is, therefore, more adequate to refer to the HOMO-derived bands as *highest occupied  $\pi$ -states* (HOPS) in these systems and to the LUMO-derived bands as the *lowest unoccupied  $\pi$ -states* (LUPS).<sup>38</sup> From Figure 8, it becomes apparent that the energy separation between the HOPS and  $E_F$ ,  $\Delta E_{HOPS}$  is completely independent of the head-group substitution (-F or -NO<sub>2</sub>) in the systems considered here.<sup>35-39, 41, 42</sup> This is consistent with our previous finding that the molecular states closer to  $E_F$  (the HOPS in this case) are *pinned* by the Fermi level.<sup>38</sup> Note that, at reduced coverage, this is no longer the case.<sup>41</sup> On the other hand, the energy separation between  $E_F$  and the LUPS,  $\Delta E_{LUPS}$ , is different for the -F and the -NO<sub>2</sub> substituted SAM, which is a consequence of the longer effective conjugation length in the latter and the strong electron accepting character of the nitro group.

The alignment of the HOPS and LUPS with  $E_F$  is given by the energy difference between  $E_F$  and the respective  $IP_{left}$  or  $EA_{left}$ , shifted by  $BD$  (Equation 3),<sup>35-39, 41, 42</sup> again, differences in  $IP_{left}$  and  $EA_{left}$  for the two adsorption scenarios, -SH and -S• (Figure 4), are compensated by the different  $BD$ s (Figure 7).

$$\Delta E_{HOPS} = \Phi_{Au} - IP_{left} + BD \quad (3.a)$$

$$\Delta E_{LUPS} = \Phi_{Au} - EA_{left} + BD \quad (3.b)$$

In fact, as the bonding-induced charge rearrangements and the resulting potential drop (Figures 6 and 7) have a tail on the first phenylene ring, the molecular electronic structure is slightly perturbed upon bonding to the metal; this has been shown to result in a small corrective term that has to be added to the right hand sides of Equations 3.<sup>35-39, 41</sup> Note that  $\Delta E_{HOPS}$  or  $\Delta E_{LUPS}$  also determine the additional tunnel barrier introduced by the SAM at the interface between electrode and organic semiconductor in an organic electronic device.

#### 4. CONCLUSION

In summary, we investigated the interface energetics in SAMs of 4'-nitro- and 4'-fluoro-4-mercaptobiphenyls on Au(111). Based on *first-principles* calculations and electrostatic reasoning, we derived a comprehensive, microscopic picture for the modification of the work function of the underlying gold substrate, the alignment of the frontier molecular orbitals in the SAM with the metal Fermi level, and the link between these two quantities. SAM formation is seen to give rise to two dipole layers. The first arises from the parallel arrangement of dipolar molecules into an ordered monolayer and leads to the observation that such a layer must have two ionization potentials and two electron affinities, one on the thiol side and one on the head-group side, respectively. The second dipole layer originates from the bond formation at the metal/SAM interface and it shifts the potential well of the SAM (and the energy levels within the SAM) relative to  $E_F$ . Together, these dipole layers determine the work-function modification and the level alignment at these interfaces and this picture holds regardless of the choice for the conceptual partitioning of the system into metallic and molecular part.

We find a strong work-function increase for the -NO<sub>2</sub> terminated layer and no considerable change of the gold work function for the -F terminated layer. Both SAMs can be expected to contribute to a lowering of the hole-injection barrier from the electrode into a subsequently deposited organic semiconductor as, even in the -F terminated case, detrimental

push-back effects at the interface between metal and active organic semiconductor are suppressed. The tunnel barrier for charge transport across the SAM, determined by the alignment of the highest occupied molecular states with  $E_F$ , does not depend on the head-group substitutions also for the systems investigated in the present study.

## ACKNOWLEDGEMENTS

GH is an INSANE Marie-Curie Fellow (contract no. 021511).

## REFERENCES

- [1] Love, J. C., Estroff, L. A., Kriebel, J. K., Nuzzo, R. G. and Whitesides, G. M., "Self-Assembled Monolayers of Thiolates on Metals as a Form of Nanotechnology," *Chem. Rev.* 105(4), 1103-1169 (2005).
- [2] Ulman, A., "Formation and Structure of Self-Assembled Monolayers," *Chem. Rev.* 96(4), 1533-1554 (1996).
- [3] Genzer, J. and Efimenko, K., "Creating Long-Lived Superhydrophobic Polymer Surfaces Through Mechanically Assembled Monolayers," *Science* 290(5499), 2130-2133 (2000).
- [4] Jennings, G. K. and Laibinis, P. E., "Self-assembled monolayers of alkanethiols on copper provide corrosion resistance in aqueous environments," *Colloids Surf., A* 116(1-2), 105-114 (1996).
- [5] Eck, W., Stadler, V., Geyer, W., Zharnikov, M., Götzhäuser, A. and Grunze, M., "Generation of Surface Amino Groups on Aromatic Self-Assembled Monolayers by Low Energy Electron Beams - A First Step Towards Chemical Lithography," *Adv. Mater.* 12(11), 805-808 (2000).
- [6] Felgenhauer, T., Yan, C., Geyer, W., Rong, H. T., Götzhäuser, A. and Buck, M., "Electrode modification by electron-induced patterning of aromatic self-assembled monolayers," *Appl. Phys. Lett.* 79(20), 3323-3325 (2001).
- [7] Geyer, W., Stadler, V., Eck, W., Zharnikov, M., Götzhäuser, A. and Grunze, M., "Electron-induced crosslinking of aromatic self-assembled monolayers: Negative resists for nanolithography," *Appl. Phys. Lett.* 75(16), 2401-2403 (1999).
- [8] Gooding, J. J., Mearns, F., Yang, W. R. and Liu, J. Q., "Self-Assembled Monolayers into the 21(st) Century: Recent Advances and Applications," *Electroanal.* 15(2), 81-96 (2003).
- [9] Halik, M., Klauk, H., Zschieschang, U., Schmid, G., Dehm, C., Schütz, M., Maisch, S., Effenberger, F., Brunnbauer, M. and Stellacci, F., "Low-voltage organic transistors with an amorphous molecular gate dielectric," *Nature* 431(7011), 963-966 (2004).
- [10] Kleineberg, U., Brechling, A., Sundermann, M. and Heinzmann, U., "STM Lithography in an Organic Self-Assembled Monolayer," *Adv. Funct. Mater.* 11(3), 208-212 (2001).
- [11] Kobayashi, S., Nishikawa, T., Takenobu, T., Mori, S., Shimoda, T., Mitani, T., Shimotani, H., Yoshimoto, N., Ogawa, S. and Iwasa, Y., "Control of carrier density by self-assembled monolayers in organic field-effect transistors," *Nat. Mater.* 3(5), 317-322 (2004).
- [12] Campbell, I. H., Kress, J. D., Martin, R. L., Smith, D. L., Barashkov, N. N. and Ferraris, J. P., "Controlling charge injection in organic electronic devices using self-assembled monolayers," *Appl. Phys. Lett.* 71(24), 3528-3530 (1997).
- [13] Campbell, I. H., Rubin, S., Zawodzinski, T. A., Kress, J. D., Martin, R. L., Smith, D. L., Barashkov, N. N. and Ferraris, J. P., "Controlling Schottky energy barriers in organic electronic devices using self-assembled monolayers," *Phys. Rev. B* 54(20), 14321-14324 (1996).
- [14] de Boer, B., Hadipour, A., Mandoc, M. M., van Woudenberg, T. and Blom, P. W. M., "Tuning of Metal Work Functions with Self-Assembled Monolayers," *Adv. Mater.* 17(5), 621-625 (2005).
- [15] Ganzorig, C., Kwak, K. J., Yagi, K. and Fujihira, M., "Fine tuning work function of indium tin oxide by surface molecular design: Enhanced hole injection in organic electroluminescent devices," *Appl. Phys. Lett.* 79(2), 272-274 (2001).
- [16] Hatton, R. A., Day, S. R., Chesters, M. A. and Willis, M. R., "Organic electroluminescent devices: enhanced carrier injection using an organosilane self assembled monolayer (SAM) derivatized ITO electrode," *Thin Solid Films* 394(1-2), 292-297 (2001).
- [17] Ihm, K., Kim, B., Kang, T. H., Kim, K. J., Joo, M. H., Kim, T. H., Yoon, S. S. and Chung, S., "Molecular orientation dependence of hole-injection barrier in pentacene thin film on the Au surface in organic thin film transistor," *Appl. Phys. Lett.* 89(3), 033504 (2006).

- [18] Yan, H., Huang, Q. L., Cui, J., Veinot, J. G. C., Kern, M. M. and Marks, T. J., "High-Brightness Blue Light-Emitting Polymer Diodes via Anode Modification Using a Self-Assembled Monolayer," *Adv. Mater.* 15(10), 835-838 (2003).
- [19] Zehner, R. W., Parsons, B. F., Hsung, R. P. and Sita, L. R., "Tuning the Work Function of Gold with Self-Assembled Monolayers Derived from X-[C<sub>6</sub>H<sub>4</sub>-C≡C-]<sub>n</sub>C<sub>6</sub>H<sub>4</sub>-SH (*n* = 0, 1, 2; X = H, F, CH<sub>3</sub>, CF<sub>3</sub>, and OCH<sub>3</sub>)," *Langmuir* 15(4), 1121-1127 (1999).
- [20] Zuppiroli, L., Si-Ahmed, L., Kamaras, K., Nüesch, F., Bussac, M. N., Ades, D., Siove, A., Moons, E. and Grätzel, M., "Self-assembled monolayers as interfaces for organic opto-electronic devices," *Eur. J. Phys. B* 11(3), 505-512 (1999).
- [21] Note that screening of the charge carriers by the metal, i.e., mirror charges or the *Schottky effect*, are not taken into account in this simplified conceptual picture.
- [22] Akkerman, H. B., Blom, P. W. M., de Leeuw, D. M. and de Boer, B., "Towards molecular electronics with large-area molecular junctions," *Nature* 441(7089), 69-72 (2006).
- [23] Akkerman, H. B., Naber, R. C. G., Jongbloed, B., van Hal, P. A., Blom, P. W. M., de Leeuw, D. M. and de Boer, B., "Electron tunneling through alkanedithiol self-assembled monolayers in large-area molecular junctions," *Proc. Natl. Acad. Sci.* 104(27), 11161-11166 (2007).
- [24] Chen, J., Reed, M. A., Rawlett, A. M. and Tour, J. M., "Large On-Off Ratios and Negative Differential Resistance in a Molecular Electronic Device," *Science* 286(5444), 1550-1552 (1999).
- [25] Elbing, M., Ochs, R., Koentopp, M., Fischer, M., von Hänisch, C., Weigend, F., Evers, F., Weber, H. B. and Mayor, M., "A single-molecule diode," *Proc. Natl. Acad. Sci.* 102(25), 8815-8820 (2005).
- [26] Jiang, P., Morales, G. M., You, W. and Yu, L. P., "Synthesis of Diode Molecules and Their Sequential Assembly to Control Electron Transport," *Angew. Chem. Int. Ed.* 43(34), 4471-4475 (2004).
- [27] Park, J., Pasupathy, A. N., Goldsmith, J. I., Chang, C., Yaish, Y., Petta, J. R., Rinkoski, M., Sethna, J. P., Abruna, H. D., McEuen, P. L. and Ralph, D. C., "Coulomb blockade and the Kondo effect in single-atom transistors," *Nature* 417(6890), 722-725 (2002).
- [28] Reed, M. A., Chen, J., Rawlett, A. M., Price, D. W. and Tour, J. M., "Molecular random access memory cell," *Appl. Phys. Lett.* 78(23), 3735-3737 (2001).
- [29] Patrone, L., Palacin, S., Charlier, J., Armand, F., Bourgoin, J. P., Tang, H. and Gauthier, S., "Evidence of the key role of metal-molecule bonding in metal-molecule-metal transport experiments," *Phys. Rev. Lett.* 91(9), 096802 (2003).
- [30] Xue, Y. Q., Datta, S. and Ratner, M. A., "Charge transfer and "band lineup" in molecular electronic devices: A chemical and numerical interpretation," *J. Chem. Phys.* 115(9), 4292-4299 (2001).
- [31] Xue, Y. Q. and Ratner, M. A., "Microscopic study of electrical transport through individual molecules with metallic contacts. I. Band lineup, voltage drop, and high-field transport," *Phys. Rev. B* 68(11), 115406 (2003).
- [32] Xue, Y. Q. and Ratner, M. A., "Microscopic study of electrical transport through individual molecules with metallic contacts. II. Effect of the interface structure," *Phys. Rev. B* 68(11), 115407 (2003).
- [33] Xue, Y. Q. and Ratner, M. A., "End group effect on electrical transport through individual molecules: A microscopic study," *Phys. Rev. B* 69(8), 085403 (2004).
- [34] Yaliraki, S. N., Kemp, M. and Ratner, M. A., "Conductance of molecular wires: Influence of molecule-electrode binding," *J. Am. Chem. Soc.* 121(14), 3428-3434 (1999).
- [35] Heimel, G., Romaner, L., Bredas, J. L. and Zojer, E., "Odd-Even Effects in Self-Assembled Monolayers of  $\omega$ -(biphenyl-4-yl)alkanethiols: A First-Principles Study," *Langmuir* 24(2), 474-482 (2008).
- [36] Heimel, G., Romaner, L., Bredas, J. L. and Zojer, E., "Interface Energetics and Level Alignment at Covalent Metal-Molecule Junctions: p-Conjugated Thiols on Gold," *Phys. Rev. Lett.* 96(19), 196806 (2006).
- [37] Heimel, G., Romaner, L., Bredas, J. L. and Zojer, E., "Organic/metal interfaces in self-assembled monolayers of conjugated thiols: A first-principles benchmark study," *Surf. Sci.* 600(19), 4548-4562 (2006).
- [38] Heimel, G., Romaner, L., Zojer, E. and Bredas, J. L., "Toward Control of the Metal-Organic Interfacial Electronic Structure in Molecular Electronics: A First-Principles Study on Self-Assembled Monolayers of  $\pi$ -Conjugated Molecules on Noble Metals," *Nano Lett.* 7(4), 932-940 (2007).
- [39] Rangger, G. M., Romaner, L., Heimel, G. and Zojer, E., "Understanding the properties of interfaces between organic self-assembled monolayers and noble metals - a theoretical perspective," *Surf. Interface Anal.*, in press (2008).
- [40] Romaner, L., Heimel, G., Gruber, M., Bredas, J. L. and Zojer, E., "Stretching and Breaking of a Molecular Junction," *Small* 2(12), 1468-1475 (2006).

- [41] Romaner, L., Heimel, G. and Zojer, E., "Electronic structure of thiol-bonded self-assembled monolayers: Impact of coverage," *Phys. Rev. B* 77(4), 045113 (2008).
- [42] Heimel, G., Romaner, L., Zojer, E. and Brédas, J. L., "The Interface Energetics of Self-Assembled Monolayers on Metals," *Acc. Chem. Res.*, to be published (2008).
- [43] Ishii, H., Sugiyama, K., Ito, E. and Seki, K., "Energy Level Alignment and Interfacial Electronic Structures at Organic/Metal and Organic/Organic Interfaces," *Adv. Mater.* 11(8), 605-625 (1999).
- [44] Kahn, A., Koch, N. and Gao, W. Y., "Electronic Structure and Electrical Properties of Interfaces between Metals and  $\pi$ -Conjugated Molecular Films," *J. Polym. Sci., Part B* 41(21), 2529-2548 (2003).
- [45] Rentenberger, S., Vollmer, A., Zojer, E., Schennach, R. and Koch, N., "UV/ozone treated Au for air-stable, low hole injection barrier electrodes in organic electronics," *J. Appl. Phys.* 100(5), 053701 (2006).
- [46] Koch, N., Duhm, S., Rabe, J. P., Vollmer, A. and Johnson, R. L., "Optimized Hole Injection with Strong Electron Acceptors at Organic-Metal Interfaces," *Phys. Rev. Lett.* 95(23), 237601 (2005).
- [47] Romaner, L., Heimel, G., Bredas, J. L., Gerlach, A., Schreiber, F., Johnson, R. L., Zegenhagen, J., Duhm, S., Koch, N. and Zojer, E., "Impact of Bidirectional Charge Transfer and Molecular Distortions on the Electronic Structure of a Metal-Organic Interface," *Phys. Rev. Lett.* 99(25), 256801 (2007).
- [48] Alloway, D. M., Hofmann, M., Smith, D. L., Gruhn, N. E., Graham, A. L., Colorado, R., Wsocki, V. H., Lee, T. R., Lee, P. A. and Armstrong, N. R., "Interface dipoles arising from self-assembled monolayers on gold: UV-photoemission studies of alkanethiols and partially fluorinated alkanethiols," *J. Phys. Chem. B* 107(42), 11690-11699 (2003).
- [49] Azzam, W., Fuxen, C., Birkner, A., Rong, H. T., Buck, M. and Wöll, C., "Coexistence of Different Structural Phases in Thioaromatic Monolayers on Au(111)," *Langmuir* 19(12), 4958-4968 (2003).
- [50] Leung, T. Y. B., Schwartz, P., Scoles, G., Schreiber, F. and Ulman, A., "Structure and growth of 4-methyl-4'-mercaptobiphenyl monolayers on Au(111): a surface diffraction study," *Surf. Sci.* 458(1-3), 34-52 (2000).
- [51] Kondoh, H., Iwasaki, M., Shimada, T., Amemiya, K., Yokoyama, T., Ohta, T., Shimomura, M. and Kono, S., "Adsorption of Thiolates to Singly Coordinated Sites on Au(111) Evidenced by Photoelectron Diffraction," *Phys. Rev. Lett.* 90(6), 066102 (2003).
- [52] Mazzarello, R., Cossaro, A., Verdini, A., Rousseau, R., Casalis, L., Danisman, M. F., Floreano, L., Scandolo, S., Morgante, A. and Scoles, G., "Structure of a CH<sub>3</sub>S Monolayer on Au(111) Solved by the Interplay between Molecular Dynamics Calculations and Diffraction Measurements," *Phys. Rev. Lett.* 98(1), 016102 (2007).
- [53] Molina, L. M. and Hammer, B., "Theoretical study of thiol-induced reconstructions on the Au(111) surface," *Chem. Phys. Lett.* 360(3-4), 264-271 (2002).
- [54] Morikawa, Y., Liew, C. C. and Nozoye, H., "Methylthiolate induced vacancy formation on Au(111): a density functional theoretical study," *Surf. Sci.* 514(1-3), 389-393 (2002).
- [55] Roper, M. G., Skegg, M. P., Fisher, C. J., Lee, J. J., Dhanak, V. R., Woodruff, D. P. and Jones, R. G., "Atop adsorption site of sulphur head groups in gold-thiolate self-assembled monolayers," *Chem. Phys. Lett.* 389(1-3), 87-91 (2004).
- [56] Woodruff, D. P., "The role of reconstruction in self-assembly of alkylthiolate monolayers on coinage metal surfaces," *Appl. Surf. Sci.* 254(1), 76-81 (2007).
- [57] Yeganeh, M. S., Dougal, S. M., Polizzotti, R. S. and Rabinowitz, P., "Interfacial Atomic-Structure of a Self-Assembled Alkyl Thiol Monolayer Au(111) - a Sum-Frequency Generation Study," *Phys. Rev. Lett.* 74(10), 1811-1814 (1995).
- [58] Yourdshahyan, Y. and Rappe, A. M., "Structure and energetics of alkanethiol adsorption on the Au(111) surface," *J. Chem. Phys.* 117(2), 825-833 (2002).
- [59] Bilic, A., Reimers, J. R. and Hush, N. S., "The structure, energetics, and nature of the chemical bonding of phenylthiol adsorbed on the Au(111) surface: Implications for density-functional calculations of molecular-electronic conduction," *J. Chem. Phys.* 122(9), 094708 (2005).
- [60] Cao, Y. P., Ge, Q. F., Dyer, D. J. and Wang, L. C., "Steric Effects on the Adsorption of Alkylthiolate Self-Assembled Monolayers on Au (111)," *J. Phys. Chem. B* 107(16), 3803-3807 (2003).
- [61] Gottschalk, J. and Hammer, B., "A density functional theory study of the adsorption of sulfur, mercapto, and methylthiolate on Au(111)," *J. Chem. Phys.* 116(2), 784-790 (2002).
- [62] Hayashi, T., Morikawa, Y. and Nozoye, H., "Adsorption state of dimethyl disulfide on Au(111): Evidence for adsorption as thiolate at the bridge site," *J. Chem. Phys.* 114(17), 7615-7621 (2001).
- [63] Morikawa, Y., Hayashi, T., Liew, C. C. and Nozoye, H., "First-principles theoretical study of alkylthiolate adsorption on Au(111)," *Surf. Sci.* 507, 46-50 (2002).

- [64] Nara, J., Higai, S., Morikawa, Y. and Ohno, T., "Density functional theory investigation of benzenethiol adsorption on Au(111)," J. Chem. Phys. 120(14), 6705-6711 (2004).
- [65] Vargas, M. C., Giannozzi, P., Selloni, A. and Scoles, G., "Coverage-dependent adsorption of CH<sub>3</sub>S and (CH<sub>3</sub>S)<sub>2</sub> on Au(111): A density functional theory study," J. Phys. Chem. B 105(39), 9509-9513 (2001).
- [66] Perdew, J. P. and Wang, Y., "Accurate and simple analytic representation of the electron-gas correlation-energy," Phys. Rev. B 45(23), 13244-13249 (1992).
- [67] Blöchl, P. E., "Projector augmented-wave method," Phys. Rev. B 50(24), 17953-17979 (1994).
- [68] Kresse, G. and Joubert, D., "From ultrasoft pseudopotentials to the projector augmented-wave method," Phys. Rev. B 59(3), 1758-1775 (1999).
- [69] Kresse, G. and Furthmüller, J., "Efficiency of ab-initio total energy calculations for metals and semiconductors using a plane-wave basis set," Comp. Mater. Sci. 6(1), 15-50 (1996).
- [70] Kresse, G. and Furthmüller, J., "Efficient iterative schemes for *ab initio* total-energy calculations using a plane-wave basis set," Phys. Rev. B 54(16), 11169-11186 (1996).
- [71] Kresse, G. and Hafner, J., "*Ab initio* molecular dynamics for liquid metals," Phys. Rev. B 47(1), 558-561 (1993).
- [72] Kresse, G. and Hafner, J., "*Ab initio* molecular-dynamics Simulation of the liquid-metal-amorphous-semiconductor transition in germanium," Phys. Rev. B 49(20), 14251-14269 (1994).
- [73] Kokalj, A., "Computer graphics and graphical user interfaces as tools in simulations of matter at the atomic scale," Comp. Mater. Sci. 28(2), 155-168 (2003).
- [74] Hasan, M., Bethell, D. and Brust, M., "The fate of sulfur-bound hydrogen on formation of self-assembled thiol monolayers on gold: H-1 NMR spectroscopic evidence from solutions of gold clusters," J. Am. Chem. Soc. 124(7), 1132-1133 (2002).
- [75] Rusu, P. C. and Brocks, G., "Surface dipoles and work functions of alkylthiolates and fluorinated alkylthiolates on Au(111)," J. Phys. Chem. B 110(45), 22628-22634 (2006).
- [76] Rusu, P. C. and Brocks, G., "Work functions of self-assembled monolayers on metal surfaces by first-principles calculations," Phys. Rev. B 74(7), 073414 (2006).
- [77] Spin-polarized (i.e., spin-unrestricted) test calculations result in the same picture, as two radicals per unit cell result in an overall closed-shell system (even number of electrons).
- [78] Chen, Y. C., Cunningham, J. E. and Flynn, C. P., "Dependence of rare-gas-adsorbate dipole-moment on substrate work function," Phys. Rev. B 30(12), 7317-7319 (1984).
- [79] Lang, N. D., "Interaction between Closed-Shell Systems and Metal-Surfaces," Phys. Rev. Lett. 46(13), 842-845 (1981).
- [80] Lang, N. D. and Kohn, W., "Theory of Metal Surfaces: Work Function," Phys. Rev. B 3(4), 1215-1223 (1971).
- [81] Witte, G., Lukas, S., Bagus, P. S. and Wöll, C., "Vacuum level alignment at organic/metal junctions: "Cushion" effect and the interface dipole," Appl. Phys. Lett. 87(26), 263502 (2005).
- [82] Koch, N., Elschner, A., Schwartz, J. and Kahn, A., "Organic molecular films on gold versus conducting polymer: Influence of injection barrier height and morphology on current-voltage characteristics," Appl. Phys. Lett. 82(14), 2281-2283 (2003).